

Further exploration of the Océ copier

Citation for published version (APA):

Sanders, R. M. W. (2003). *Further exploration of the Océ copier*. (DCT rapporten; Vol. 2003.028). Technische Universiteit Eindhoven.

Document status and date:

Published: 01/01/2003

Document Version:

Publisher's PDF, also known as Version of Record (includes final page, issue and volume numbers)

Please check the document version of this publication:

- A submitted manuscript is the version of the article upon submission and before peer-review. There can be important differences between the submitted version and the official published version of record. People interested in the research are advised to contact the author for the final version of the publication, or visit the DOI to the publisher's website.
- The final author version and the galley proof are versions of the publication after peer review.
- The final published version features the final layout of the paper including the volume, issue and page numbers.

[Link to publication](#)

General rights

Copyright and moral rights for the publications made accessible in the public portal are retained by the authors and/or other copyright owners and it is a condition of accessing publications that users recognise and abide by the legal requirements associated with these rights.

- Users may download and print one copy of any publication from the public portal for the purpose of private study or research.
- You may not further distribute the material or use it for any profit-making activity or commercial gain
- You may freely distribute the URL identifying the publication in the public portal.

If the publication is distributed under the terms of Article 25fa of the Dutch Copyright Act, indicated by the "Taverne" license above, please follow below link for the End User Agreement:

www.tue.nl/taverne

Take down policy

If you believe that this document breaches copyright please contact us at:

openaccess@tue.nl

providing details and we will investigate your claim.

Further exploration of the Océ copier

R.M.W.Sanders

DCT nr. 2003.28

Supervisor:
dr.ir. M.J.G. van de Molengraft

Section Dynamics and Control Technology
Faculty Mechanical Engineering
University of Technology Eindhoven

Eindhoven, May 2003

Summary

Nowadays it is unthinkable to live in a world without copiers. The customers expect increasing performance of a copier. This results in a machine with complex mechanical components. The copier that is relevant for this research is an 8445 copier of Océ. This copier can be divided into three main units namely the Organic Photo Conductor unit (OPC), the Toner Transfer Fusion unit (TTF) and the Paper Feed unit. The copy of the original document appears for the first time on the OPC belt and will from there be transported via the TTF belt to the out going paper.

During the transport of the image on the OPC belt arise different problems that have to be solved. The OPC unit consist of several cylinders, which cannot be placed exact parallel to each other. This causes a displacement of the OPC belt in axial direction. The belt finally can hit the copier frame and will be damaged. The installation of a steering roller solves this problem in combination with a controller. Another problem appears when the OPC belt and the TTF belt making contact with each other. Both units are driven by two different motors. It is not possible that both motors give exactly the same velocity to each belt, there are always small deviations. To compensate for these small errors OCE has introduced a yoke. The installation of the yoke turned out to be not necessary afterwards, when a functional controller is used. One control strategy seems to be a serious option for implementation, namely Iterative Learning Control (ILC). Because the copier is set up of cyclic components and the interaction between these components causes errors that are expected to have a cyclic behaviour. This is suitable for ILC. Therefore a case study of ILC is worked out, to illustrate how ILC can be used and implemented on the copier in future research projects.

Table of contents

<i>Summary</i>	1
<i>Table of contents</i>	2
<i>Introduction</i>	3
<i>Chapter 1: Copier description</i>	4
1.1 OPC unit	4
1.2 TTF unit	7
1.3 Paper Feed unit	8
<i>Chapter 2: Copier interface</i>	9
2.1 Interface	9
2.2 Sensors	10
2.3 Motors	12
<i>Chapter 3: Iterative Learning Control</i>	13
3.1 ILC theory	13
3.2 ILC Simulation	14
<i>Chapter 4: Recommendations and conclusion</i>	17
4.1 Recommendations	17
4.2 Conclusion	17
<i>Bibliography</i>	18
<i>Appendix 1: Copier layout</i>	19
<i>Appendix 2: Physical network</i>	20
<i>Appendix 3: LMD 18200 H-Bridge</i>	21
<i>Appendix 4: OPC initialisation</i>	27
<i>Appendix 5: OPC controller</i>	28
<i>Appendix 6: Opto-Switch</i>	29
<i>Appendix 7: OCE Drive section</i>	31
<i>Appendix 8: ILCfile.m</i>	32
<i>Appendix 9: ILCsim.mdl</i>	34

Introduction

There are many manufacturers of copiers in the world and OCE is one of them. Every manufacturer has his own ideas about the technical aspects inside the machine, but the main idea of all the manufacturers is making many and quick copies. The targets are designing a copier that can copy as much as possible copies in as few as possible time. Control engineers can tackle many problems that can contribute to the optimisation of the copier. The OCE copier contains three main units namely the OPC unit, the TTF unit and the Paper Feed unit that are all components with a cyclic behaviour. This will possibly lead to a special behaviour of the errors and this is again a challenge for the engineers. The copier that is used in this research is a stripped down OCE 8445 copier, with only the necessary components on it.

The main goals of this research are creating an orderly and fully equipped line-up of the copier and making an inventory of the opportunities with Iterative Learning Control.

This report starts with a description of the working principles of the OCE copier and a few specific problems. In Chapter 2 is described the copier interface and the hardware components that are indispensable to get an operational copier. The problems encountered during the installation of some hardware components are also discussed and worked out. Errors are expected to be cyclic, because the main units in the copier are also cyclic of nature. One control strategy that is suitable for such problems is Iterative Learning Control. A theoretical overview and a simulation of ILC is given in Chapter 3. Recommendations for further research are made in Chapter 4 and also conclusions are drawn about this research.

Chapter 1: Copier description

In this chapter will be explained the working principles of the OCE copier with respect to the three main units. The three units are respectively the Organic Photo Conductor unit (OPC), the Toner Transfer Fusion unit (TTF) and the Paper Feed unit. A side view of the OCE copier with names of machine parts is presented in appendix 1, *Copier Layout*.

1.1 OPC unit

The OPC unit consists of 7 cylinders over which an organic photo conductor belt moves, see appendix 1. The OPC unit is driven by a controllable engine M_01 , which is joined to W_01 with an rubber-indented belt. The working velocity of the OPC belt lies during normal use between 0.2 m/s and 0.5 m/s.

The beginning of every new working cycle starts with making a digital image of the original document, which lies on top of the copier. The image is projected on the organic photo conductor belt in the next stage. The projection of the image on the OPC belt is made possible, because OCE has developed a belt with special properties. The main property of the new belt is his sensitivity for light. When the belt is locally exposed, this will lead to a locally magnetised part of the OPC belt. Making use of this property the image can be applied on the belt by exposing those places of the belt where later on the image must appear. A row of LED's is used to expose the OPC belt. These LED's change in time to project the image on the moving OPC belt.

The second stage within the OPC unit starts when the magnetised belt passes the toner supply unit, W_05 . Toner particles have the same properties in a magnetic field as iron particles. So the magnetic OPC belt attracts the toner particles from the toner supply unit and on the OPC belt will the image be formed with toner particles. The toner unit delivers the toner particles on a specific way to the OPC belt. Inside the toner supply cylinder that delivers the toner are placed magnets. These magnets cause for a specific pattern of toner particles as shown in *fig 1.1, placement of the toner particles*.

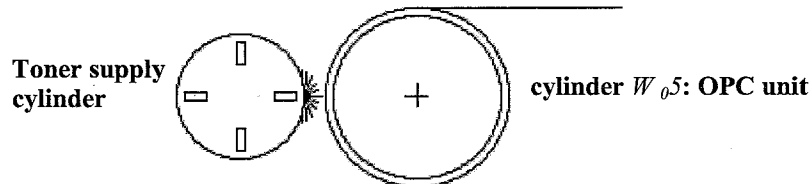


fig 1.1, placement of the toner particles

Because of the specific pattern, only the toner particles those who stand up straight will be place on the OPC belt. This leads to an optimal placement of the toner particles. One remark has to be made about the strength of the magnets in the toner supply cylinder. The strength of the magnetic field in the toner supply cylinder is weaker than the magnetic force on the OPC belt. If this is not true, then there is no transportation of toner particles. So toner transportation is only guaranteed if the magnetic force of the OPC belt is stronger than the magnetic field on the toner supply cylinder.

The image of the original document is now rendered into a toner image on the OPC belt. The transfusion of the toner particles from the OPC unit to the TTF unit is the last stage, with exception of the cleaning stage of the OPC belt, before the working cycle begins again. The material type of the TTF belt is different from the OPC belt. The TTF belt is made of rubber, which is a complete different material than the OPC belt. There are two requirements to guarantee a sufficient transfusion of toner. The temperature and the contact pressure at the contact point of the two belts need to be high enough. The temperature must lie between 90°C and 100°C. At this temperature the toner particles melt and prefer to stick on the rubber belt of the TTF unit instead of the OPC belt. The OPC belt is cleaned at W_07 after the transfusion process and is now ready to record a new image.

1.1.1 Clamp mechanism

The photo conductor belt and the TTF belt are not always clamped together during a working cycle. For this reason a clamp mechanism, see *fig 1.2 Clamp mechanism*, is made to clamp or release the belts. It is possible to lift up the OPC-roller against the TTF belt using an eccentric, which is driven by a motor. The spring is attached to the eccentric to guarantee a sufficiently high clamp force, when the

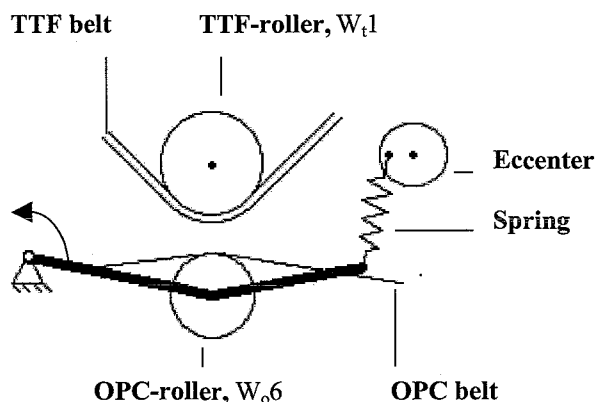


fig 1.2, clamp mechanism

OPC roller is lifted up. A brake is fixed to the rotor of the eccentric motor. This brake can be activated when the required clamp force is reached. The clamp mechanism is not operational at the moment, because in this stage of the research of the copier it is not necessary to have a fully operational clamp mechanism. It is possible to clamp the OPC roller on the TTF belt also by manual operation. The wheel that is indicated by a white arrow in figure 1.3 is called the eccentric wheel. With the eccentric wheel it is possible to make a manual lift up of the OPC cylinder, W_6 . The brake at the rotor motor is not installed, so a solution has to be made to replace the brake function. In the eccentric wheel are six holes, which can be used for a provisionally solution. Turning the eccentric wheel tightens the spring in the clamp mechanism. Putting a cylinder in one of the holes such that no rotation of the eccentric is possible can hold the mechanism in the up position. In this way it is possible to clamp the TTF belt against the OPC belt.

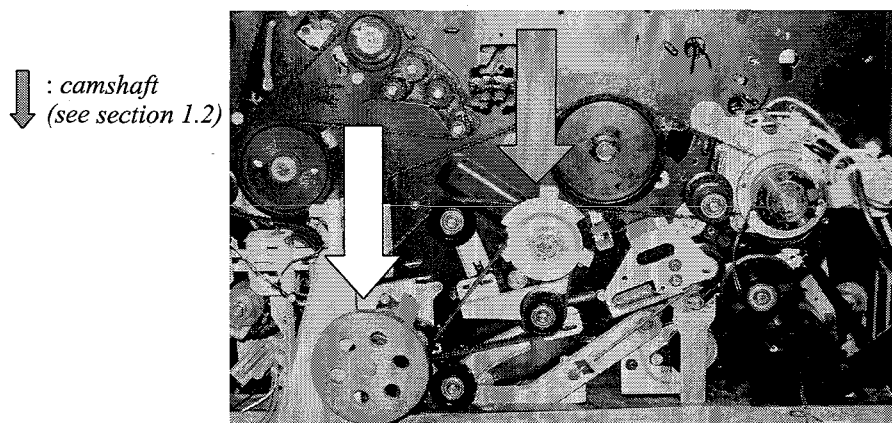


fig 1.3, Eccentric wheel (back of the copier)

1.1.2 Steering roller

The OPC unit consists as mentioned earlier of 7 cylinders. These cylinders cannot be placed perfect parallel to each other, due to imperfections occurred during the assembling and manufacturing stages. The not completely parallel cylinders lead to an axial displacement of the OPC belt. The OPC belt runs slowly of the cylinders and will hit the copier frame, if this displacement is not corrected. OCE has installed a steering roller that can compensate for displacements of the OPC belt in axial direction. One end of the steering roller can be displaced in upward direction, perpendicular to the axial displacement direction of the OPC belt (see figure 1.4).

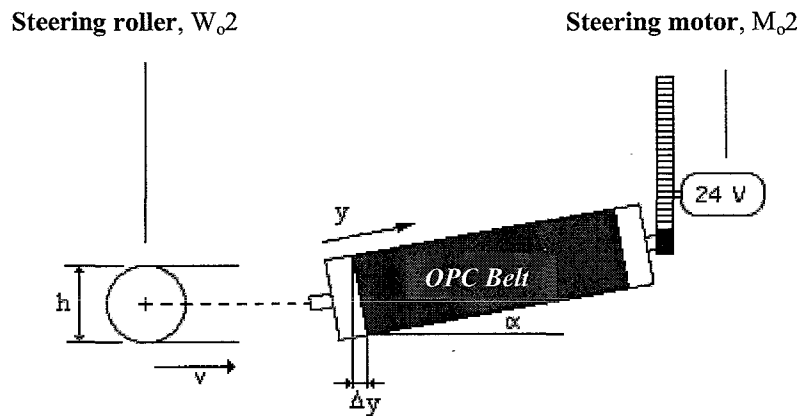


fig 1.4, Steering principle OPC unit

It is possible to control the axial movement of the OPC belt, because a controllable motor M_{02} drives an indented strip that moves the cylinder end up or down. The maximum stroke, which can be realised, is 35 mm. The left sketch (in fig 1.4) of the steering roller is a side view, seen from the fixed cylinder end in positive y direction. The displacement of the OPC belt Δy can be calculated with the formula standing below:

$$\Delta y = h \cdot \sin(\alpha) \tag{1}$$

The whole belt must pass the steering roller before the belt is moved up with Δy . The variables used in formula (1) and figure 1.4 are declared in table 1.1

Δy	The displacement of the belt	[m]
h	The arc length, that is in contact with the steering roller	[m]
α	The slope of the steering roller with the ground level	[rad]
v	The velocity of the OPC belt	[m/s]

Table 1.1, Declaration of the variables

1.1.3. Speed differences

The projection of the image on the OPC belt must take place during a constant velocity of the belt, because disturbances leads to incorrect projection such as to much space between the lines. The OPC belt and the TTF belt are both driven by two different motors. It is not possible that both motors give exactly the same velocity to each belt, there are always small deviations. To compensate for these small errors OCE has introduced a yoke, which connects the cylinders W_{03} and W_{04} . The yoke can

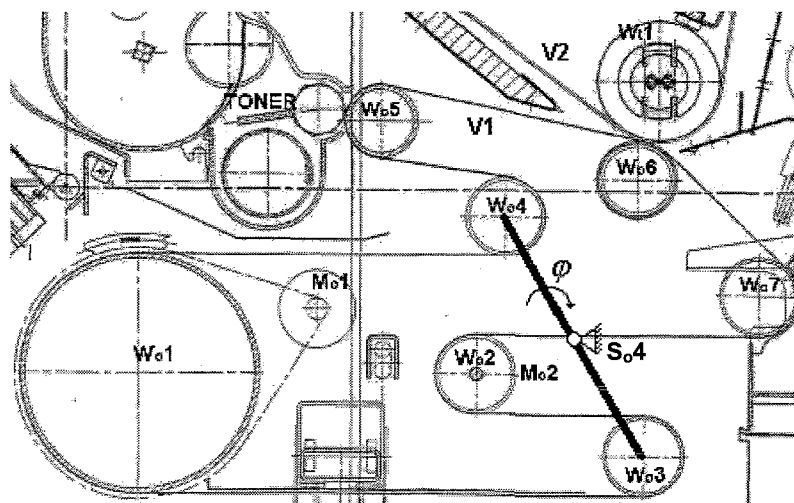


fig 1.5, Speed difference compensation by means of a yoke

rotate around the indicated joint on which a potential meter $S_{0,4}$ is fixed, see fig 1.5. In here are V_1 and V_2 respectively the velocities of the OPC motor and the TTF motor. The potential meter measures the angle rotation of the yoke. When the OPC motor runs a little bit faster as the TTF motor, the OPC belt wants to fold itself up before the contact point $W_{0,6}$. After the contact point the OPC belt wants to stretch out. Rotating the yoke in positive φ direction can make a compensation for this behaviour. When the TTF motor runs faster as the OPC motor, the OPC belt folds after the contact point and stretches before the contact point. In this situation the yoke must rotate in negative φ direction. A stiffer TTF belt material causes the fold and stretch behaviour of the OPC belt.

After the design stage of the copier, OCE discovered that the yoke is not necessary at all. But it was too late to change the yoke and replace it by a control strategy, which can solve the problem also.

The simplest model that describes a relation between the angular velocity of the yoke and the speed difference is presented in formula (2). A few assumptions are made to come to model in formula (2) namely:

- No slip is present in the contact point and in the drive parts.
- No friction model is present in the system.
- The sine of a small angle φ is equal to φ .

$$\Delta v = v_1 - v_2 = \frac{\Delta x}{\Delta t} = \frac{R \cdot \sin(\Delta\varphi)}{\Delta t} = \frac{\Delta\varphi \cdot R}{\Delta t} = \dot{\varphi} \cdot R \Rightarrow \dot{\varphi} = \frac{v_1 - v_2}{R} \rightarrow \text{Integrator} \quad (2)$$

The yoke is in fact a mechanical controller with a feedback of the speed differences. With control techniques of today it should be possible to replace it by a controller. In figure 1.6 is presented a block

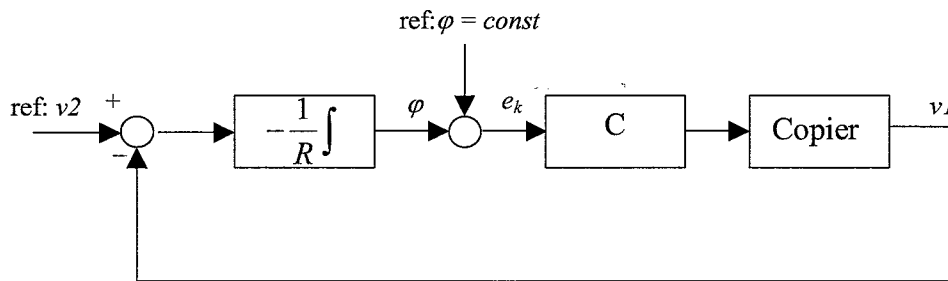


fig 1.6, Blockscheme Copier

scheme with a feedback. This is presented as an indication how a block scheme of the copier with a controller look likes. One assumption is made with respect to the average of the speed difference signal. The signal is assumed to have an average of zero, if this turns out to be not true. Then an extra controller has to be introduced before the integrator action.

1.2 TTF unit

A non-controllable main motor that is fixed on the backside of the copier drives the Toner Transfer fusion unit. The TTF unit consists of three main cylinders on which a rubber belt moves counter clockwise. Comparing the TTF unit with the OPC unit no steering roller is needed, because the rubber belt of the TTF unit is more flexible. The axial displacement of the rubber belt is corrected in the machine by placing little barrier plates that push the rubber belt back in the right direction.

The second image transition takes place at $W_{1,2}$, where the TTF unit meets the Paper Feed unit. As seen earlier there is not always a physical contact between the OPC unit and the TTF unit. For the TTF unit and the paper feed unit this is the same. Therefore a camshaft N1 is installed in the TTF unit. The camshaft end can be seen in figure 1.3 indicated by a blue arrow. On the camshaft are placed three different cams. The most important cam determines whether there is contact between the TTF and the Paper Feed unit. The other two cams are not relevant because they take care for the lift of two cleaning cylinders and the cleaning process is no issue in this assignment. The cleaning cylinders are placed against $W_{1,3}$. The camshaft can be divided in three states namely standby, waiting and run. The run state is the only state in which the Paper Feed unit is in contact with the TTF unit. To set the camshaft in the run state a little physical force is needed. In general a rubber-indented belt drives the camshaft,

which is driven by the same motor as the clamp mechanism of the OPC unit. In this case everything must take place manually.

Back to the transition of the image from the TTF unit to the Paper Feed unit. The transition is a transition from a rubber to paper. Due to the pre-heated paper and the high pressure in the contact point the toner particles prefer to stick on the paper. The TTF belt is cleaned after the transition and is ready again to take up toner particles from the OPC belt.

1.3 Paper Feed unit

The last stage in the copier process is the Paper Feed unit. The main motor that drives the TTF unit is also the driver for the Paper Feed unit. The paper enters at cylinder W_p1 , where also the pre-heating of the paper starts. The pre-heating is essential for the transition of the toner particles to the paper. When no heating of the paper is present the toner particles get stuck on the TTF belt and no image will appear on the exported copy. After the contact point at cylinder W_p3 the paper goes immediately to output rack where the user can see the result of his copy.

Chapter 2: Copier interface

An interface is a unit composed of hardware and software parts, which gives the user the possibility to operate and observe a physical system. The interface pertaining to the OCE copier and the hardware components that are needed to get a working copier are explained in this chapter. For a complete overview of the physical connections of the hardware is referred to appendix 2, *Physical Network*.

2.1 Interface

2.1.1 Hardware

A Dspace hardware unit enables generating and capturing of signals to and from the OCE copier. The Dspace hardware consists of a processor board DS1003 in combination with two I/O boards, namely DS2002 and DS4002. The DS2002 I/O board is only used to receive signals from the angle sensor S_{o4} and the velocity sensor TTF, S_{t1} . The DS4002 board has more functions and one of them is to receive signals from the tape sensor S_{o3} , the encoder sensor S_{o1} and the hole sensor S_{o2} . The DS4002 board is not only used to receive signals, but also capable of generating high frequency pulse signals for the driver unit. The method of using high frequency pulses for steering a motor is called Pulse Width Modulation (PWM). A pulse pattern with a fixed frequency is used instead of supplying a continuous constant voltage. The used pulse frequencies for the motors in the copier are 2000 kHz. This frequency can be changed a little as long as the motor runs without shocks. The frequency is not the only adjustable parameter, because the duty cycle can also be adjusted. The duty cycle has influence on the effective delivered voltage, because the duty cycle is defined as the pulse width divided through the pulse period.

These PWM signals are sent to the LMD18200 H-bridges, designed by National Semiconductor for driving motors with PWM. These H-bridges need as input a direction signal and a PWM signal to drive a motor. The direction only indicates in which direction the motor must turn, to the left is 0 and to the right is 1. Every H-bridge has 4 connections: connection 1 and 4 are the connections to the motor over where a voltage difference has to be created. Connection 2 and 3 are the connections with the DS4002 board, which represent respectively the input for the PWM signal and the direction signal of the motor. More detailed information about the LMD18200 H-bridges can be found in appendix 3.

2.1.2 Software

During the modelling stage can be made use of the program Matlab 5.3, with the simulink toolbox. The real time adjustments can be done with the Dspace software Controldesk. The required files are stored at the computer belonging to the OCE copier, in the folder c:\users\copier. In here are standing folders with files for the initialisation (opcinit) of the steering roller and the controller (opcregelbaar) of the steering roller. In the following paragraphs of 2.1.2 shall be explained shortly the working of the initialisation and controller.

2.1.2.1 Initialisation

The former initialisation did not work correctly. The steering roller has to go to a starting position from where the controller can take in control, but this position was not correct. The idea behind the initialisation is to move the steering roller up in the top position and move than back down during a fixed time as long as the steering roller is in the right starting position. When the steering roller arrives in the top position a tapping noise arises. This is the intention and after a few seconds the steering roller will move down during 15 seconds and the initialisation is finished. The simulink file of the initialisation is added in appendix 4.

2.1.2.2 Controller

The controller has to achieve that the OPC belt does not move of the steering roller. The whole controller, [2], is based on the tape sensor signal, because this signal influences the direction and the duty cycle of the steering motor. The steering motor changes namely in opposite direction, when the tape sensor changes. For example if the sensor signal changes from 0 to 1 the direction of the steering motor changes from 1 to 0. In this way the tape sensor continues with seeking the edge of the OPC belt every time again. The sensor influences as said also the duty cycle, but only when the steering

roller is moving longer as 3 seconds. The steering motor stops after a movement of three seconds and waits till the tape sensor signal changes of sine. The OPC motor runs above all always in positive direction, with a duty cycle of 0.3. The simulink file of the controller is added in appendix 5.

2.2 Sensors

In the original configuration of the copier only opto-switch sensors were used to register information. Opto-switches are photosensitive sensors consisting of two parts standing right in front of each other. One part generates a light signal with a LED and the opposite part, a photodiode, tries to receive this light. The output signal of the opto-switch is high if an object is placed between the LED and the photodiode. In other circumstances when no object is between it, the output signal is low. All the opto-switch sensors are connected to the sensor circuit, which is supplied by the main supply 220 V - 50Hz. For documentation about the Opto-switch is referred to appendix 6. The function description of every specific opto-switch sensor on the copier will now be explained.

Encoder sensor, S_{o1}

Motor M_{o1} drives cylinder W_{o1} by a rubber belt. The rotation of this cylinder can be registered by an opto-switch in combination with an encoder ring. The encoder ring is fixed on the outer radius of the cylinder W_{o1} and contains 465 small holes, this means a resolution of 0.77 degrees. A resolution of 0.77 degrees implies a displacement of the OPC belt of 1 mm.

Hole sensor, S_{o2}

The hole sensor opto-switch is fixed at the lowest level of the OPC belt behind the main cylinder W_{o1} . The opto-switch sensor can be used to measure the cycle time of the OPC belt. One part of the sensor is placed under the OPC belt and the other part is placed above. The cycle time can be measured, because there is made a hole in the OPC belt on the spot of the sensor. The output signal will change every time when the hole passes the opto-switch.

Tape sensor, S_{o3}

As earlier mentioned displaces the OPC belt in axial direction. The tape sensor, which observes the displacement is fixed before W_{o3} and is placed in such a way that the edge of the OPC belt is detected when the belt axially moves.

Angle sensor, S_{o4}

Another type of sensor is used to register the angle rotation of the yoke. In the former configuration an opto-switch sensor was placed to detect the rotation. An opto-switch sensor is not suitable, because an opto-switch has only the output signals 0 and 1. The options for installing a new sensor were an inductive sensor and a potential meter. Both sensors are suitable but the final choice is made for the potential meter. The potential meter is a little bit cheaper, but the main argument is that the potential meter is much easier to fix onto the yoke. The output signal of the potential meter lies between 0.15 and 0.3 volts.

Velocity sensor TTF, S_{t1}

On the main motor M_{t1} are already fixed three unknown feedback wires. One of these feedback wires turned out to be a velocity sensor. A calibration has to be executed before the velocity sensor can be used adequately. For the calibration are taken five run-configurations in to account. During each run-configuration was measured the voltage difference and the angle velocity using a velocity meter. A line fit is applied on the measured data, to see if there is a relation between the angle velocity and the supplied voltage. The relation can be estimated with a linear function. The results are presented in table 2.1 and figure 2.1. The reduced voltage difference is the signal, which is captured in Dspace.

Run-configuration	Voltage difference [V]	Reduced voltage difference [V]	Angle velocity [rad/s]
standing still	0	0	0
TTF and paper unit with camshaft in run position	5,5	3,1	14,1
TTF and paper unit with camshaft not in run position	5,8	3,3	14,8
Rubber drivebelt is the only load	16,8	9,4	43,0
unloaded run	17,3	9,7	44,3

Table 2.1, Calibration results

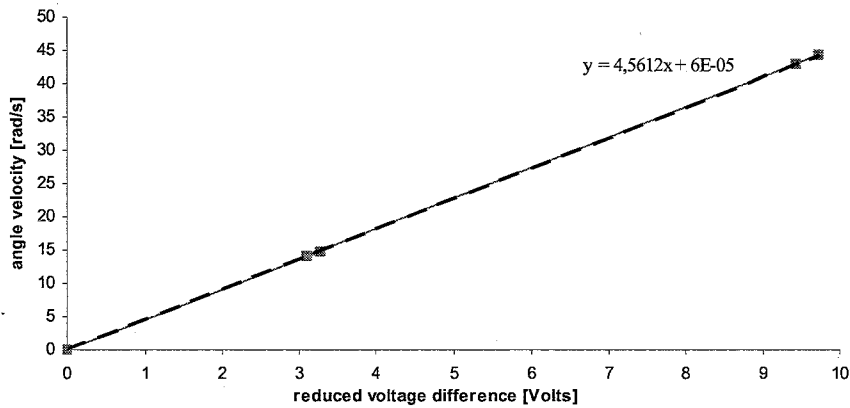


fig 2.1, Calibration of the angle velocity sensor

The angle velocity of the main motor is the measured voltage multiplied by the factor 4.56. The DS2002 board receives the signal of the angle velocity, but this signal must not be higher than 10 Volts. Initially the maximum supplied voltage difference was 17.3 Volts, see table 2.1 column voltage difference. This is much too high and therefore the following electrical scheme is installed to create an input signal for the Dspace 2002 board that is lower than 10 Volt, see table 2.1 column reduced voltage difference. The new reduced voltage difference is now a factor 1,78 smaller.

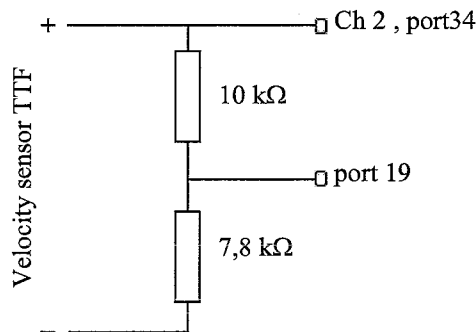


fig 2.2, Electrical scheme to reduce the signal of the velocity sensor TTF

2.3 Motors

Different motors are installed on the copier, but they are not connected all at the moment. Four motors are used in the current running copier, three of them are controllable and one is not. The functions of each motor and specific information are explained in the following paragraphs of section 2.3.

2.3.1 OPC motor, M_{o1}

The OPC motor is a controllable motor and drives the OPC tape using a rubber-indented belt. Running velocities of the OPC belt lie between 0.2 m/s and 0.5 m/s. The motor is fixed on the right side besides the W_{o1} cylinder. The OPC motor is supplied by a 24 V power source.

2.3.2 Steering motor, M_{o2}

The function of the controllable steering motor, as mentioned earlier in paragraph 1.1.2, is driving a plastic strip, which lifts the steering roller for making a displacement correction of the OPC belt. The steering motor is also supplied by a 24 V power source and is fixed close to the yoke on the left side. Velocities of the steering motor are not known, but an estimation of the moving velocity of the steering roller can be made between a 0.1 cm/s and 0.2 cm/s.

2.3.3 Sensor motor, M_{o3}

Up to now was assumed that tape sensor S_{o3} has one fixed position to find the edge of the OPC belt. Sensor motor M_{o3} is controllable and has the possibility to move the tape sensor head in axial direction. On the sensor motor is fixed a cam that causes a stroke of maximally 5 mm in axial direction. The voltage supply for the Sensor motor is 24 Volts.

2.3.4 TTF motor, M_i1

The TTF motor is a non-controllable motor and drives, using a rubber-indented belt, the TTF unit and the Paper Feed unit. A schematic overview of the OCE drive section, seen from the back of the copier, is added in appendix 7. The rubber belt that was essential to make an operational TTF and Paper Feed unit is called in here the maindrive system. The TTF motor must originally be supplied with 190 Volts, but for non-continuous use of the TTF motor it is also possible to supply the motor with 220 Volts. The motor becomes rather hot when running on 220 Volts, but it is only for temporal use. For driving the TTF unit and Paper Feed unit a reasonably high torque is needed. The motor had initially not enough power to get the units running. A capacitor of 6 μ F is installed to help the motor in the beginning, with starting the copier units. The TTF motor is fixed on the back of the copier above the W_{o1} cylinder and its usual running velocities are about 14 rad/s.

Chapter 3: Iterative Learning Control

OCE has installed a yoke to compensate for small speed differences between the OPC and TTF unit. Later on it turned out to be not necessary to install a yoke, because with the use of a controller it should be possible to drive the OPC motor M_{o1} in such way that the speed difference can be hold nearly zero and the yoke stands still. In the copier are placed several units that are all based on a specific cycle. The several units have interaction with each other and the errors resulting from this interaction may be cyclic of nature. A serious control option for this problem is possibly Iterative Learning Control (ILC). Input of the system is the electrical potential of the OPC motor and the tracking error is the rotation of the yoke. In this research it was not possible to implement ILC on the copier, because of less time. Therefore an ILC simulation of another system is made to give an indication how ILC can be implemented on the copier, [1] and [4].

3.1 ILC theory

An important requirement to guarantee good results with ILC is that the systematic errors must be greater as the random errors. ILC is based on a feed-forward signal that is designed by an off-line iteration process. This process stores and re-uses the error information to come to an improvement of the tracking performance. A schematical block scheme of ILC is represented in fig 3.1.

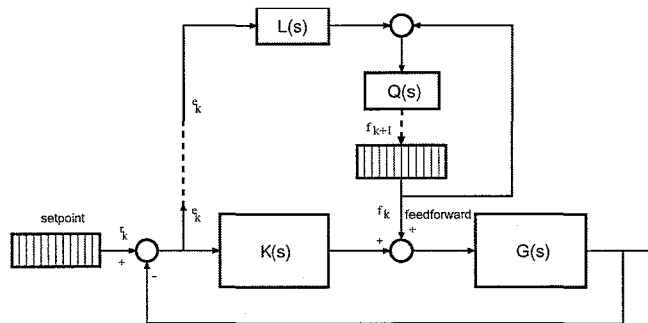


fig 3.1, Block scheme ILC

In here are K and G respectively the controller and the plant. L and Q are both filters and e_k is the error signal at sample k .

The feedback of this block scheme can be represented as:

$$e_k = \frac{-G}{1+GK} f_k \quad (3)$$

The ILC feedforward is represented as:

$$f_{k+1} = Q(f_k + L \cdot e_k) \quad (4)$$

Making use of relation (3) and (4) leads to a relation in which f is eliminated:

$$\begin{aligned} e_{k+1} &= \frac{-G}{1+GK} \cdot f_{k+1} \\ &= \frac{-G}{1+GK} \cdot Q(f_k + L \cdot e_k) \\ &= Q \left(1 + \frac{-G}{1+GK} \cdot L \right) e_k \end{aligned} \quad (5)$$

There is convergence of relation (5) if the following relation satisfies. Relation (6) is called the convergence criterion.

$$\left| Q \left(1 - \frac{G}{1 + GK} \cdot L \right) \right| < 1 \quad (6)$$

From the convergence criterion can be seen that the error goes to zero immediately, when the L filter is chosen equal to the inverse process-sensitivity. Designing an L filter that is equal to the inverse process-sensitivity is difficult if the inverse process-sensitivity goes to infinity for $\omega \rightarrow \infty$ and if the process-sensitivity is non-minimum phase. Q is an anti-causal and low-pass filter and is used to create more robustness for modelling errors. This robustness filter is designed such that it suppresses the frequency components at which the plant model is inaccurate. The lower frequencies at which the model is correct are passed through the robustness filter.

3.2 ILC Simulation

ILC cannot be implemented on the copier and a frequency response function is needed to implement it. Therefore an example frequency response function is used to explain the ILC implementation in steps. Injecting noise on the OPC motor input and measuring the velocity of the OPC belt results in a frequency response function of the copier. The OPC motor must run on a constant speed when noise is injected. The considered system in this simulation is a rotating motor with a position measurement. Input of the system is the electrical potential of the motor and output is the angle rotation of a mass at the output shaft. The goal of the simulation is to follow a reference trajectory with high precision. Available for this ILC simulation are a measured frequency response function and the matching frequency vector of the considered system.

The frequency response function is fitted with **frfit** (fig 3.2), because with **frfit** it is possible to write the system in matrix representation as follows.

$$[Ap, Bp, Cp, Dp] = \text{frfit}(frf, hz, [12, 10, 2], 1)$$

Frif is the frequency response data and *hz* is the matching frequency vector. The numbers 12, 10 and 2 between the brackets representing respectively the number of poles, zeros and integrators which are needed for creating a reliable fit. Number 1 indicates that a weighting function $\text{inv}(\text{abs}(frf))$ is used.

frf data (blue), current estimation (green), previous estimation (red)

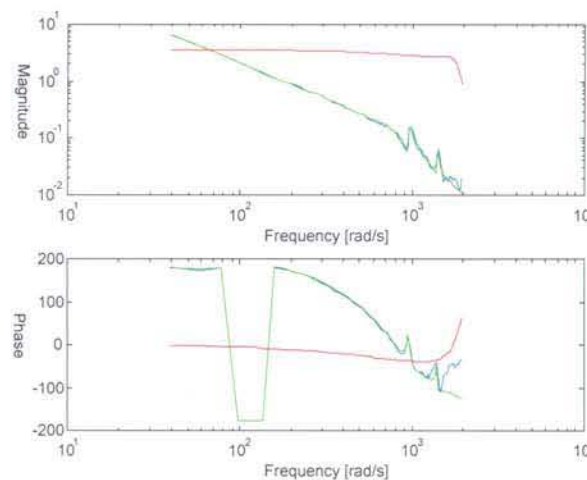


fig 3.2, fit results of the frf function

The matrices must be made global before they can be loaded in Diet, [3]. With Diet it is possible to add a simple controller, which later can be imported in simulink just like the matrices A_p , B_p , C_p and D_p . A lead/lag controller is chosen, which leads to a chosen bandwidth of 10 Hz.

The real ILC part starts with designing a learning filter L . The first step in designing an L-filter starts with making a calculation of the process-sensitivity, $S_p = G/(1+KG)$, in num/den representation. This calculation can be done making use of the model and controller in num/den representation. The obtained transfer function must be minimised with **minreal**. This results in a model where all uncontrollable or unobservable modes have been removed. The new minimised transfer function is subsequently been discretised with **c2dm** on 1 kHz. Discretisation is needed for using **zpetc**. Zpetc determines a stable estimation of the inverse of the process-sensitivity, but zpetc causes a few samples delay, *phd*, to result in a causal filter. Compensation for the delay must be made after the filter is used.

The compensation is made in the time domain by setting back the time of the obtained vector by *phd* samples, in the frequency domain is the compensation made by adding positive phase as follows [5]:

$$phase(L(\omega)) = phase(L(\omega)) + (\omega \cdot phd \cdot T_s) \quad (7)$$

Filtering the error can now be done with the created L-filter and using **filter**. The filtered error L_e is correct when the data is set back over *phd* samples.

Designing a Q filter is the next step in the ILC procedure. Q must be a low-pass filter and filtering itself must take place anti-causal. A low-pass filter is designed with **butter** and anti-causal filtering takes place with **filtfilt**. Filfilt must filter the sum of L_e and the old feedforward F as follows:

$$F_n = Q(F + L_e) \quad (8)$$

In figure 3.3 are represented the results of ILC during 4 iterations. The original maximum error was 0.1247 rad and the maximum error after the ILC simulation is $2.37 \cdot 10^{-5}$ rad. This is a considerable improvement. So the use of ILC is worthwhile in this simulation. The convergence criterion is also checked and satisfies, because it is always smaller as 1. The results of the convergence criterion are plotted in figure 3.4. Using ILC on the copier is expected to have also a positive effect on the speed difference effect, cyclic error expectations. But results depend on size of the random errors relative to the systematic error. ILC cannot compensate for random errors.

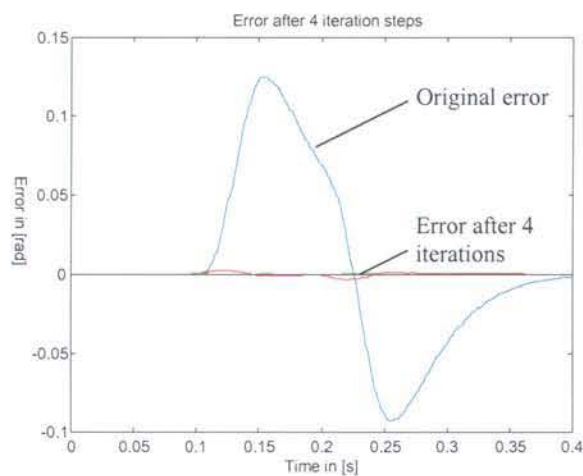


fig 3.3, Error during 4 iteration using ILC

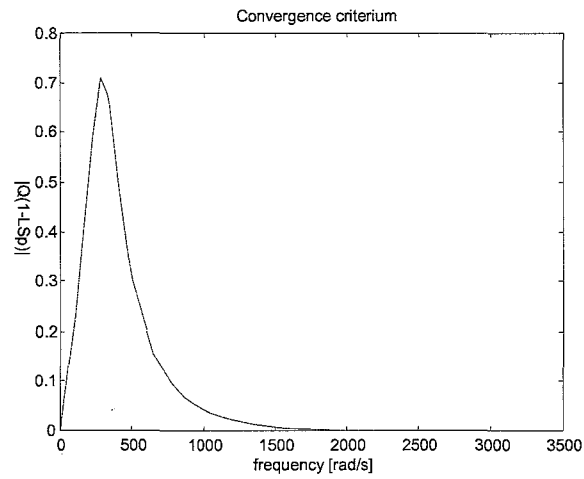


fig 3.4, Convergence criterium

The results of the simulation are made using the matlab and simulink files *ILCfile.m* and *ILCsim.mdl*. These files are presented respectively in appendix 8 and 9.

Chapter 4: Recommendations and conclusion

4.1 Recommendations

There are a few points that deserve some attention in future researches.

- One of them is the yoke mechanism. The yoke is not necessary in the copier profile, when a functional controller is implemented. An assignment can be to design a controller that makes the yoke standing still during operation. A recommendable controller for future use is discussed in chapter 3 namely an Iterative Learning Controller.
- The steering roller is controlled using the information read by an opto-switch sensor. This sensor is not optimal because it sends only a 0 or a 1 signal. In future can be thought about using another sensor that can follow for example a certain fluorescent or reflecting line on the OPC belt.
- The TTF unit is made operational using an uncontrollable motor, M_1 . The possibilities of installing a controllable motor can be investigated.

4.2 Conclusion

The beginning of this research on the OCE copier was partly practically. In this stage of the research, the copier is reconnected and cleaned up into an orderly workstation for future use.

A controller for the steering mechanism of the OPC unit is developed in the previous research project [2]. Before the controller of the steering roller could work correctly, a few adjustments were made to the initialisation file of the steering roller mechanism. The former initialisation file placed the steering roller in the lowest start position, which is wrong.

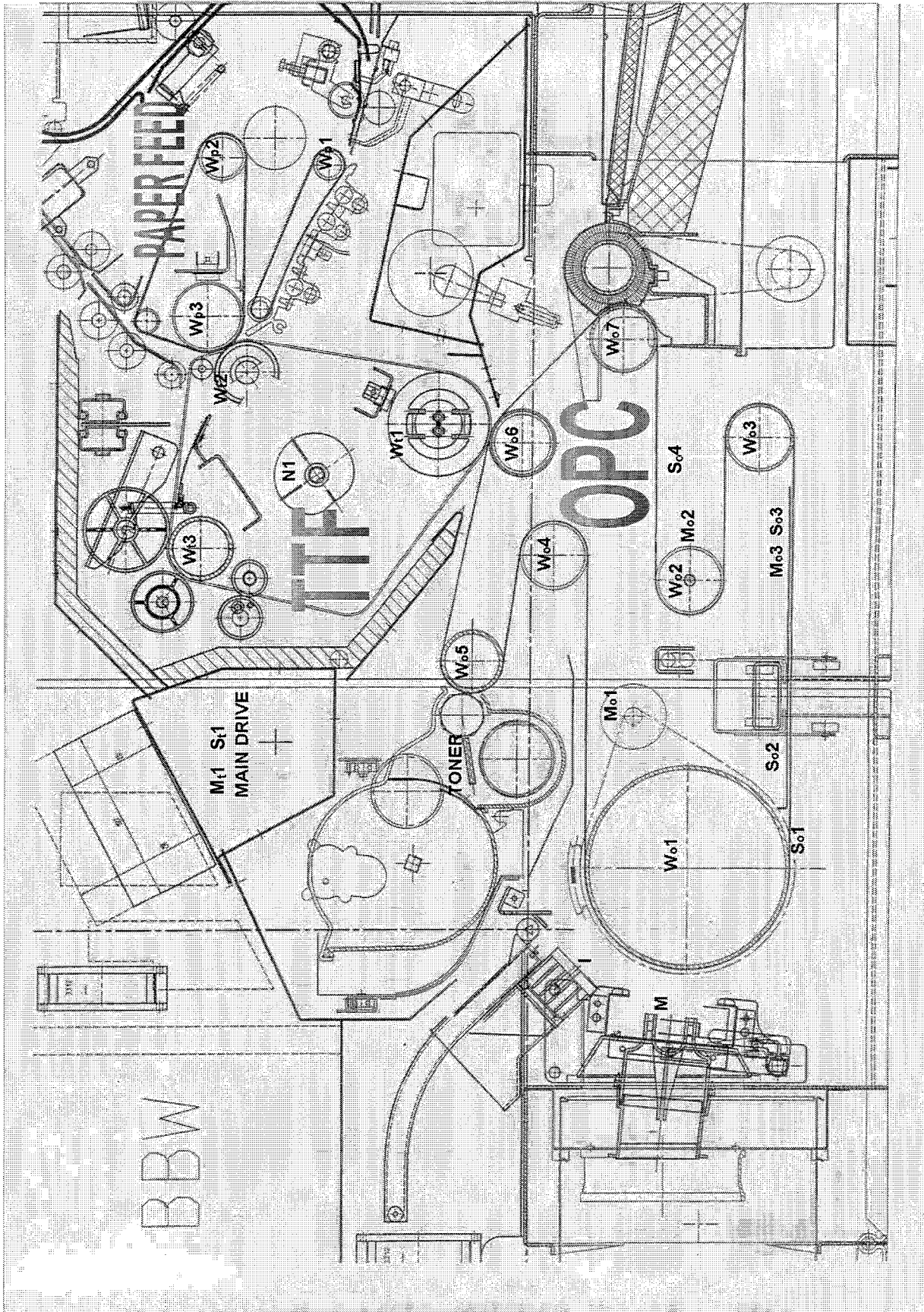
The TTF unit and the Paper Feed unit are two important parts in the copier. These two units are made operational by installing the specific drive belt of OCE and a main drive motor. The originally supply for the main drive motor is 190 Volt, but for temporal use it is possible to supply it with 220 Volts. Besides the main drive is also installed an angle sensor on the yoke of the OPC unit. The installation of the angle sensor is done, to give the next researcher the opportunity to design a controller that can compensate for speed differences between the OPC unit and the TTF unit.

The possibilities using an ILC strategy can be a serious option for future use. The copier is build out of cyclic components and the interaction between these components causes errors. These errors are expected also to be cyclic of nature.

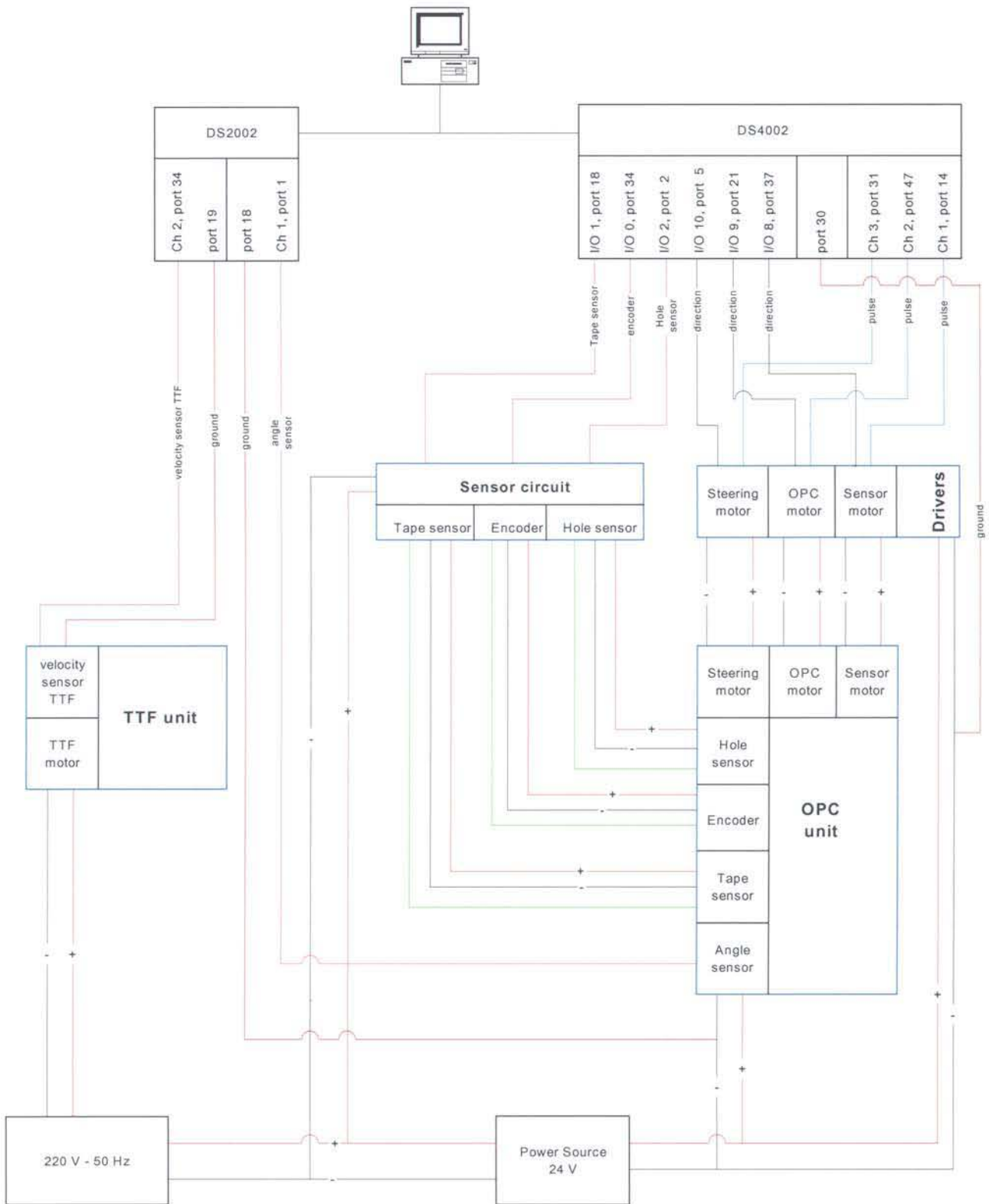
Bibliography

- [1] Documentation Iterative Learning Control course *Capita Selecta in Control* (4K140) by Prof.dr.ir.M.Steinbuch and Dr.ir. H.A. van Essen, 2002.
- [2] v.d.Boogaert, E.A.H.F., *Océ Copier*, DCT no. 2001.63
- [3] The Do It Easy Tool (DIET) is a program, which facilitates the design and tuning of controllers. For more information contact Prof.dr.ir.M.Steinbuch: m.steinbuch@tue.nl
- [4] Hendriks, S.G.M., *Iterative Learning Control on the H-drive*, DCT no. 2000.37
- [5] Franklin, G.F., Powell, J.D., Emami-Naeini, A., *Feedback Control of Dynamic Systems*, Third edition. MA: Addison-Wesley, 1994.

Appendix 1: Copier layout

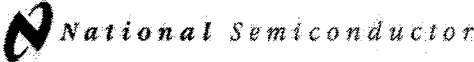


Appendix 2: Physical network



Appendix 3: LMD 18200 H-Bridge

December 1999



LMD18200 3A, 55V H-Bridge

General Description

The LMD18200 is a 3A H-Bridge designed for motion control applications. The device is built using a multi-technology process which combines bipolar and CMOS control circuitry with DMOS power devices on the same monolithic structure. Ideal for driving DC and stepper motors, the LMD18200 accommodates peak output currents up to 6A. An innovative circuit which facilitates low-loss sensing of the output current has been implemented.

- No "shoot-through" current
- Thermal warning flag output at 145°C
- Thermal shutdown (outputs off) at 170°C
- Internal clamp diodes
- Shorted load protection
- Internal charge pump with external bootstrap capability

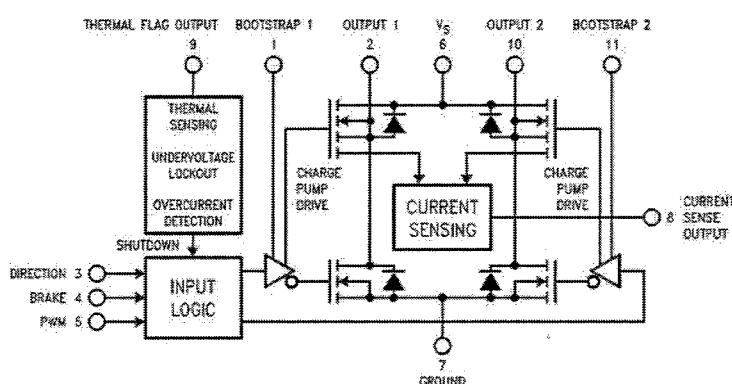
Features

- Delivers up to 3A continuous output
- Operates at supply voltages up to 55V
- Low $R_{DS(ON)}$ typically 0.3 Ω per switch
- TTL and CMOS compatible inputs

Applications

- DC and stepper motor drives
- Position and velocity servomechanisms
- Factory automation robots
- Numerically controlled machinery
- Computer printers and plotters

Functional Diagram



The diagram shows the internal architecture of the LMD18200. It features an INPUT LOGIC block with three inputs: DIRECTION (pin 3), BRAKE (pin 4), and PWM (pin 5). This block is connected to a central H-bridge circuit. The H-bridge consists of four MOSFETs (two N-channel and two P-channel) and four diodes. The output nodes are labeled OUTPUT 1 (pin 2) and OUTPUT 2 (pin 10). The supply voltage V_S is connected to pin 6, and GROUND is pin 7. A THERMAL SENSING block (pin 9) and an OVERCURRENT DETECTION block (pin 8) are also shown. The diagram includes labels for CHARGE PUMP DRIVE and CURRENT SENSE OUTPUT.

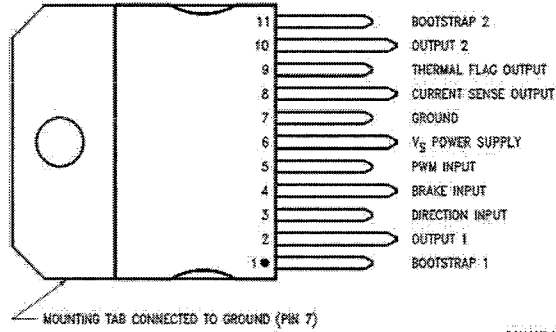
FIGURE 1. Functional Block Diagram of LMD18200

DS010568-1

LMD18200 3A, 55V H-Bridge

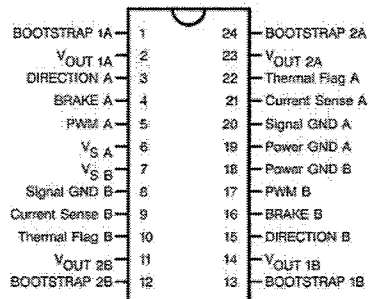
LMD18200

Connection Diagrams and Ordering Information



ts901089-2

11-Lead TO-220 Package
Top View
Order Number LMD18200T
See NS Package TA11B



ts901089-2S

24-Lead Dual-in-Line Package
Top View
Order Number LMD18200-2D-QV
5962-9232501VXA
LMD18200-2D/883
5962-9232501MXA
See NS Package DA24B

Absolute Maximum Ratings (Note 1)

If Military/Aerospace specified devices are required, please contact the National Semiconductor Sales Office/ Distributors for availability and specifications.

Total Supply Voltage (V_S , Pin 6)	60V
Voltage at Pins 3, 4, 5, 8 and 9	12V
Voltage at Bootstrap Pins (Pins 1 and 11)	$V_{OUT} + 16V$
Peak Output Current (200 ms)	6A
Continuous Output Current (Note 2)	3A
Power Dissipation (Note 3)	25W

Power Dissipation ($T_A = 25^\circ C$, Free Air)	3W
Junction Temperature, $T_{J(max)}$	150°C
ESD Susceptibility (Note 4)	1500V
Storage Temperature, T_{STG}	-40°C to +150°C
Lead Temperature (Soldering, 10 sec.)	300°C

Operating Ratings(Note 1)

Junction Temperature, T_J	-40°C to +125°C
V_S Supply Voltage	+12V to +55V

Electrical Characteristics (Note 5)

The following specifications apply for $V_S = 42V$, unless otherwise specified. **Boldface** limits apply over the entire operating temperature range, $-40^\circ C \leq T_J \leq +125^\circ C$, all other limits are for $T_A = T_J = 25^\circ C$.

Symbol	Parameter	Conditions	Typ	Limit	Units
$R_{DS(ON)}$	Switch ON Resistance	Output Current = 3A (Note 6)	0.33	0.4/0.6	Ω (max)
$R_{DS(ON)}$	Switch ON Resistance	Output Current = 6A (Note 6)	0.33	0.4/0.6	Ω (max)
V_{OLAMP}	Clamp Diode Forward Drop	Clamp Current = 3A (Note 6)	1.2	1.5	V (max)
V_{IL}	Logic Low Input Voltage	Pins 3, 4, 5		-0.1	V (min)
I_{IL}	Logic Low Input Current	$V_{IN} = -0.1V$, Pins = 3, 4, 5		-10	μA (max)
V_{IH}	Logic High Input Voltage	Pins 3, 4, 5		2	V (min)
I_{IH}	Logic High Input Current	$V_{IN} = 12V$, Pins = 3, 4, 5		10	μA (max)
	Current Sense Output	$I_{OUT} = 1A$ (Note 6)	377	325/300	μA (min)
				425/450	μA (max)
	Current Sense Linearity	$1A \leq I_{OUT} \leq 3A$ (Note 7)	± 6	± 9	%
	Undervoltage Lockout	Outputs Turn OFF		9	V (min)
				11	V (max)
T_{JW}	Warning Flag Temperature	Pin 9 $\leq 0.8V$, $I_L = 2 mA$	145		$^\circ C$
$V_F(ON)$	Flag Output Saturation Voltage	$T_J = T_{JW}$, $I_L = 2 mA$	0.15		V
$I_F(OFF)$	Flag Output Leakage	$V_F = 12V$	0.2	10	μA (max)
T_{JSD}	Shutdown Temperature	Outputs Turn OFF	170		$^\circ C$
I_S	Quiescent Supply Current	All Logic Inputs Low	13	25	mA (max)
t_{don}	Output Turn-On Delay Time	Sourcing Outputs, $I_{OUT} = 3A$ Sinking Outputs, $I_{OUT} = 3A$	300		ns
t_{on}	Output Turn-On Switching Time	Bootstrap Capacitor = 10 nF Sourcing Outputs, $I_{OUT} = 3A$ Sinking Outputs, $I_{OUT} = 3A$	100		ns
			80		ns
t_{doff}	Output Turn-Off Delay Times	Sourcing Outputs, $I_{OUT} = 3A$ Sinking Outputs, $I_{OUT} = 3A$	200		ns
			200		ns
t_{off}	Output Turn-Off Switching Times	Bootstrap Capacitor = 10 nF Sourcing Outputs, $I_{OUT} = 3A$ Sinking Outputs, $I_{OUT} = 3A$	75		ns
			70		ns
t_{pw}	Minimum Input Pulse Width	Pins 3, 4 and 5	1		μs
t_{cpr}	Charge Pump Rise Time	No Bootstrap Capacitor	20		μs

LMD18200

Electrical Characteristics Notes

Note 1: Absolute Maximum Ratings indicate limits beyond which damage to the device may occur. DC and AC electrical specifications do not apply when operating the device beyond its rated operating conditions.

Note 2: See Application Information for details regarding current limiting.

Note 3: The maximum power dissipation must be derated at elevated temperatures and is a function of $T_{j(max)}$, $R_{\theta(jc)}$, and T_c . The maximum allowable power dissipation at any temperature is $P_{D(max)} = (T_{j(max)} - T_c)/R_{\theta(jc)}$, or the number given in the Absolute Ratings, whichever is lower. The typical thermal resistance from junction to case ($R_{\theta(jc)}$) is 1.0°C/W and from junction to ambient ($R_{\theta(ja)}$) is 30°C/W. For guaranteed operation $T_{j(max)} = 125^\circ\text{C}$.

Note 4: Human-body model, 100 pF discharged through a 1.5 kΩ resistor. Except Bootstrap pins (pins 1 and 11) which are protected to 1000V of ESD.

Note 5: All limits are 100% production tested at 25°C. Temperature extreme limits are guaranteed via correlation using accepted SQC (Statistical Quality Control) methods. All limits are used to calculate AOQL (Average Outgoing Quality Level).

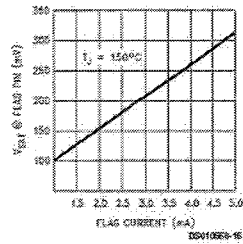
Note 6: Output currents are pulsed ($t_w < 2\text{ms}$, Duty Cycle $< 5\%$).

Note 7: Regulation is calculated relative to the current sense output voltage with a 1A load.

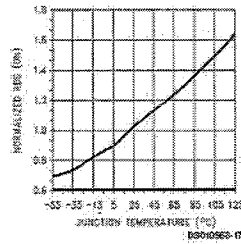
Note 8: Selections for tighter tolerance are available. Contact factory.

Typical Performance Characteristics

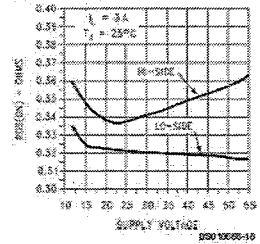
V_{SAT} vs Flag Current



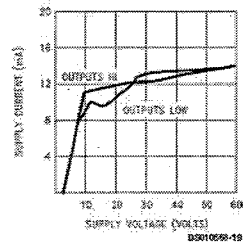
R_{DS(ON)} vs Temperature



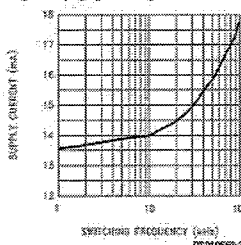
R_{DS(ON)} vs Supply Voltage



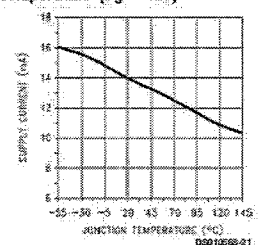
Supply Current vs Supply Voltage



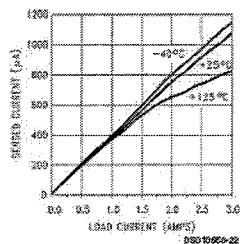
Supply Current vs Frequency (V_S = 42V)



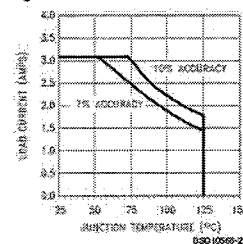
Supply Current vs Temperature (V_S = 42V)



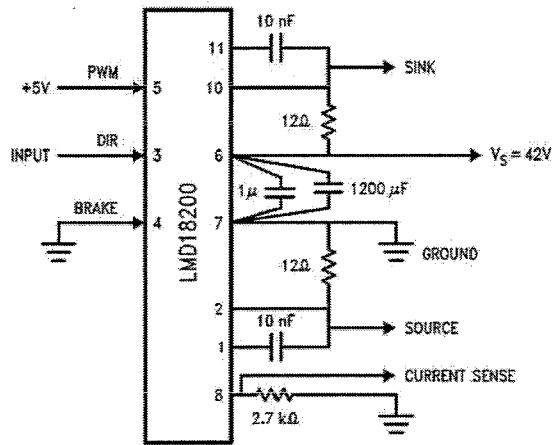
Current Sense Output vs Load Current



Current Sense Operating Region

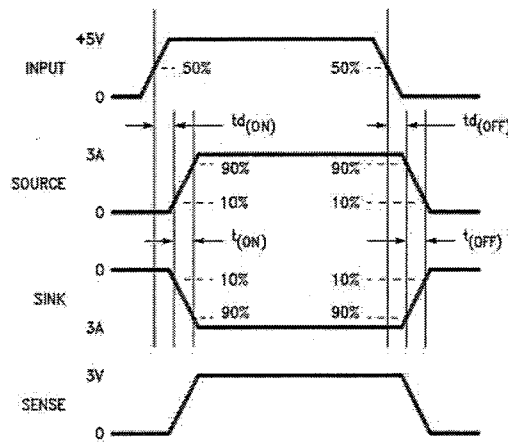


Test Circuit



0501066-8

Switching Time Definitions



0501066-8

Pinout Description (See Connection Diagram)

Pin 1, BOOTSTRAP 1 input: Bootstrap capacitor pin for half H-bridge number 1. The recommended capacitor (10 nF) is connected between pins 1 and 2.

Pin 2, OUTPUT 1: Half H-bridge number 1 output.

Pin 3, DIRECTION input: See Table 1. This input controls the direction of current flow between OUTPUT 1 and OUTPUT 2 (pins 2 and 10) and, therefore, the direction of rotation of a motor load.

Pin 4, BRAKE input: See Table 1. This input is used to brake a motor by effectively shorting its terminals. When braking is desired, this input is taken to a logic high level and

it is also necessary to apply logic high to PWM input, pin 5. The drivers that short the motor are determined by the logic level at the DIRECTION input (Pin 3): with Pin 3 logic high, both current sourcing output transistors are ON; with Pin 3 logic low, both current sinking output transistors are ON. All output transistors can be turned OFF by applying a logic high to Pin 4 and a logic low to PWM input Pin 5; in this case only a small bias current (approximately -1.5 mA) exists at each output pin.

Pin 5, PWM input: See Table 1. How this input (and DIRECTION input, Pin 3) is used is determined by the format of the PWM signal.

LMD18200

Pinout Description

(See Connection Diagram) (Continued)

Pin 6, V_S Power Supply

Pin 7, GROUND Connection: This pin is the ground return, and is internally connected to the mounting tab.

Pin 8, CURRENT SENSE Output: This pin provides the sourcing current sensing output signal, which is typically 37.7 μ A/A.

Pin 9, THERMAL FLAG Output: This pin provides the thermal warning flag output signal. Pin 9 becomes active-low at 145°C (junction temperature). However the chip will not shut itself down until 170°C is reached at the junction.

Pin 10, OUTPUT 2: Half H-bridge number 2 output.

Pin 11, BOOTSTRAP 2 Input: Bootstrap capacitor pin for Half H-bridge number 2. The recommended capacitor (10 nF) is connected between pins 10 and 11.

TABLE 1. Logic Truth Table

PWM	Dir	Brake	Active Output Drivers
H	H	L	Source 1, Sink 2
H	L	L	Sink 1, Source 2
L	X	L	Source 1, Source 2
H	H	H	Source 1, Source 2
H	L	H	Sink 1, Sink 2
L	X	H	NONE

Application Information

TYPES OF PWM SIGNALS

The LMD18200 readily interfaces with different forms of PWM signals. Use of the part with two of the more popular forms of PWM is described in the following paragraphs.

Simple, locked anti-phase PWM consists of a single, variable duty-cycle signal in which is encoded both direction and amplitude information (see Figure 2). A 50% duty-cycle PWM signal represents zero drive, since the net value of voltage (integrated over one period) delivered to the load is zero. For the LMD18200, the PWM signal drives the direction input (pin 3) and the PWM input (pin 5) is tied to logic high.

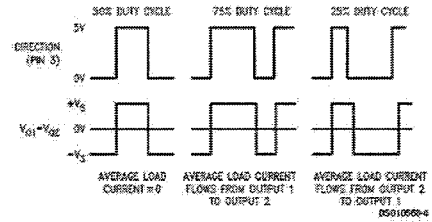


FIGURE 2. Locked Anti-Phase PWM Control

Sign/magnitude PWM consists of separate direction (sign) and amplitude (magnitude) signals (see Figure 3). The (absolute) magnitude signal is duty-cycle modulated, and the absence of a pulse signal (a continuous logic low level) represents zero drive. Current delivered to the load is proportional to pulse width. For the LMD18200, the DIRECTION input (pin 3) is driven by the sign signal and the PWM input (pin 5) is driven by the magnitude signal.

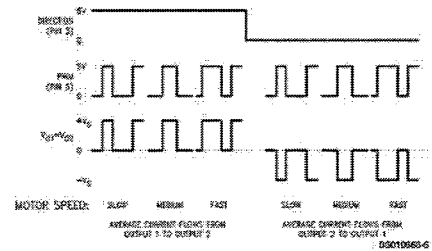
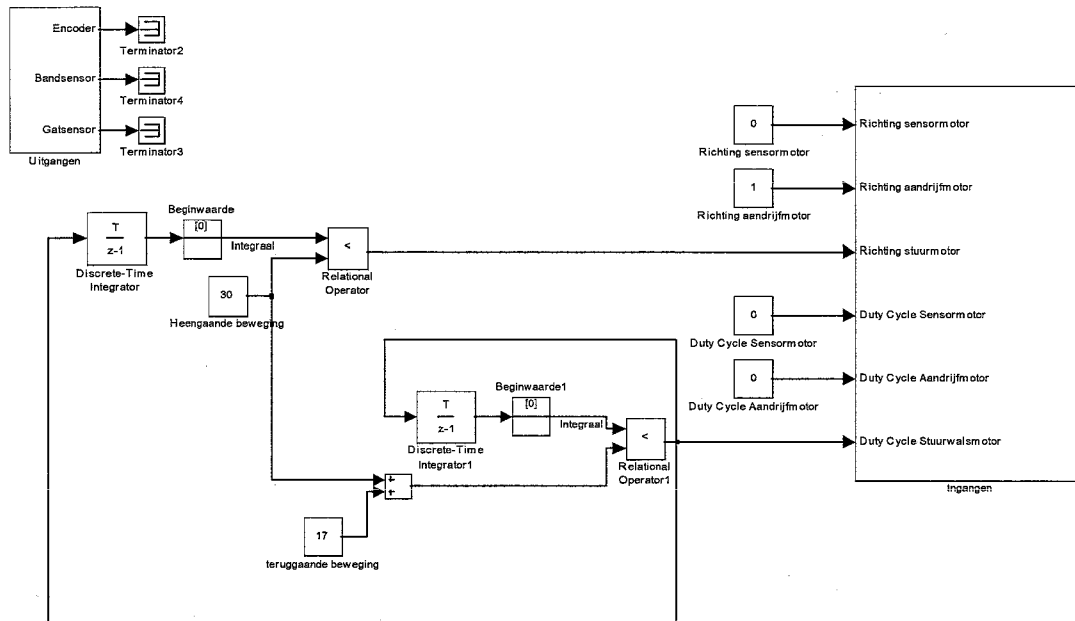


FIGURE 3. Sign/Magnitude PWM Control

SIGNAL TRANSITION REQUIREMENTS

To ensure proper internal logic performance, it is good practice to avoid aligning the falling and rising edges of input signals. A delay of at least 1 μ s should be incorporated between transitions of the Direction, Brake, and/or PWM input signals. A conservative approach is to be sure there is at least 500ns delay between the end of the first transition and the beginning of the second transition. See Figure 4.

Appendix 4: OPC initialisation



Appendix 6: Opto-Switch

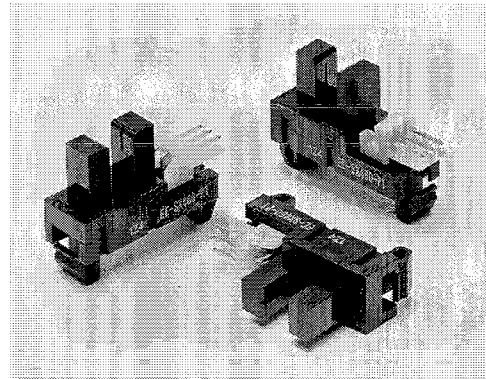
OMRON

Opto-Switch

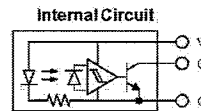
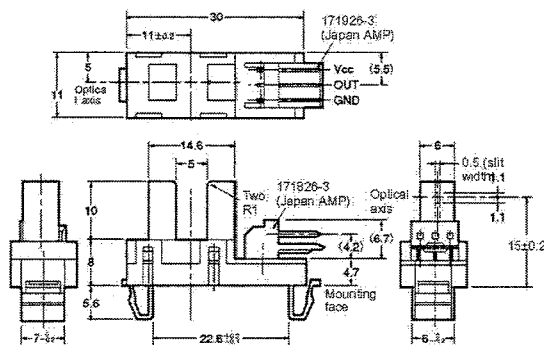
EE-SX460-P1

Transmissive

- Photo-IC output.
- Snap-in mounting model.
- Mounts to 0.8- to 1.6-mm-thick panels.
- With a 5-mm-wide slot.
- Photo IC output signals directly connect to C-MOS and TTL.
- Connects to Omron EE-1005 and AMP's EI series connectors



Dimensions



Terminal No.	Name
V	Supply voltage (Vcc)
O	Output (OUT)
G	Ground (GND)

Unless otherwise specified, the tolerances are as shown below.

Dimensions	Tolerance
3 mm max.	±0.3
3 < mm ≤ 6	±0.375
6 < mm ≤ 10	±0.45
10 < mm ≤ 18	±0.55
18 < mm ≤ 30	±0.65

Recommended Connectors:
 Japan AMP 171922-3 (crimp-type connector)
 172142-3 (crimp-type connector)
 OMRON EE-1005 (with harness)

Specifications

Absolute Maximum Ratings (Ta = 25°C)

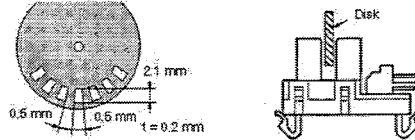
Item	Symbol	Rated value
Supply voltage	V _{CC}	10 V
Output voltage	V _{OUT}	28 V
Output current	I _{OUT}	16 mA
Permissible output dissipation	P _{OUT}	250 mW (see note)
Operating temperature	T _{OP}	-20°C to 75°C
Storage temperature	T _{STG}	-40°C to 85°C
Soldering temperature	T _{SO}	—

Note: Refer to the temperature rating chart if the ambient temperature exceeds 25°C.

■ Electrical and Optical Characteristics (Ta = 25°C, VCC = 5 V±10%)

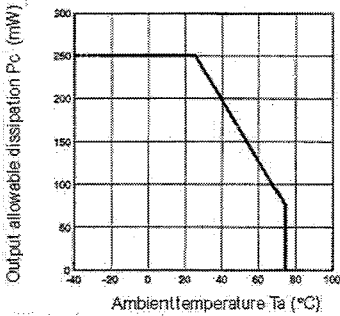
Item	Symbol	Value	Condition
Current consumption	I _{CC}	30 mA max.	With and without incident
Low-level output voltage	V _{OL}	0.3 V max.	I _{OUT} = 16 mA with incident
High-level output voltage	V _{OH}	(V _{CC} × 0.9) V min.	V _{OUT} = V _{CC} without incident, R _L = 47 kΩ
Response frequency	f	3 kHz min.	V _{OUT} = V _{CC} , R _L = 47 kΩ (see note)

Note: The value of the response frequency is measured by rotating the disk as shown below.

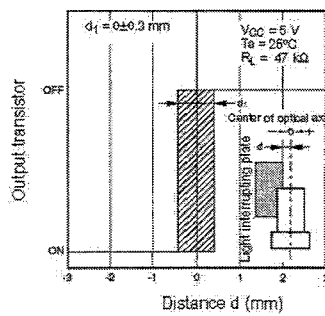


Engineering Data

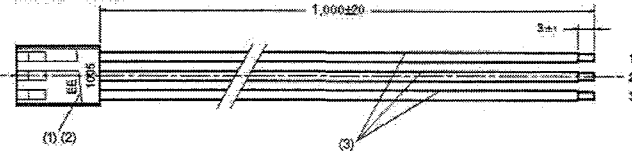
Output Allowable Dissipation vs. Ambient Temperature Characteristics



Sensing Position Characteristics (Typical)



EE-1005 Connector

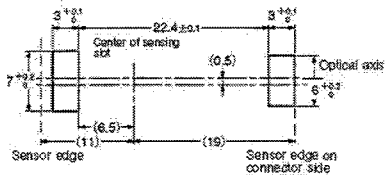


No.	Name	Model	Quantity	Maker
1	Receptacle housing	171822-3	1	Japan AMP
2	Receptacle contact	170262-1	3	Japan AMP
3	Lead wire	UL1007 AWG24	3	---

Wiring

Connector circuit no.	Lead wire color
1	Red
2	Orange
3	Yellow

■ Recommended Mounting Hole Dimensions and Mounting and Dismounting Method



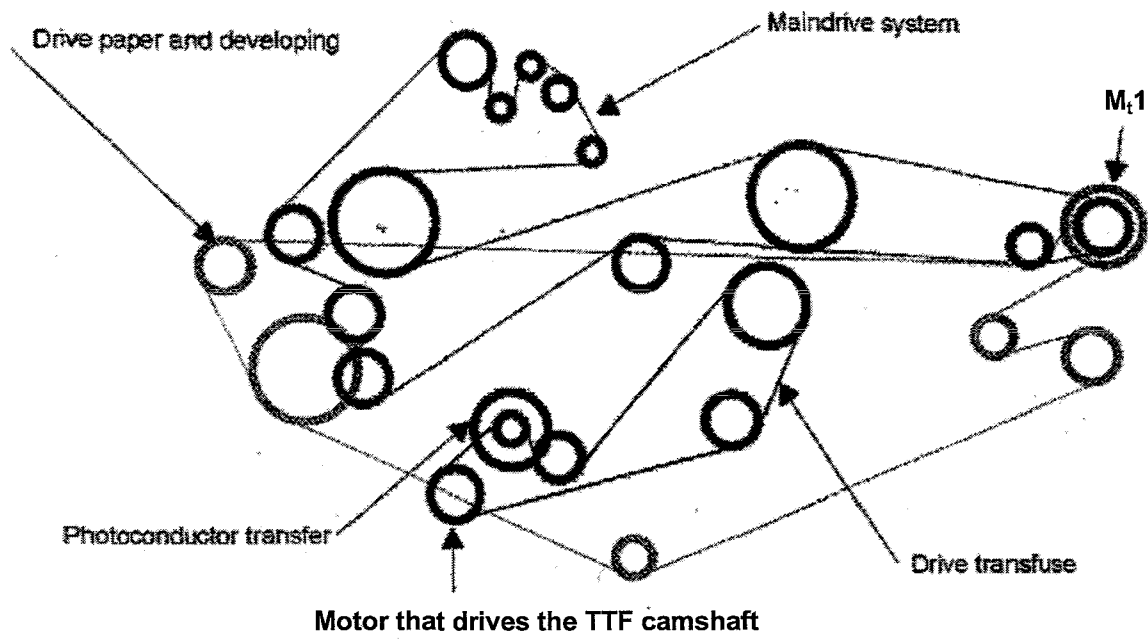
The Opto-Switch can be mounted to 0.8- to 1.6-mm-thick panels.

Refer to the above mounting hole dimensions and open the mounting holes in the panel to which the Opto-Switch will be mounted.

Insert into the holes the Opto-Switch's mounting portions with a force of three to five kilograms but do not press in the Opto-Switch at one time. The Opto-Switch can be easily mounted by inserting the mounting portions halfway and then slowly pressing the Opto-Switch onto the panel.

Dismounting is achieved by either hand (below panel), or screwdriver (above panel).

Appendix 7: OCE Drive section



Appendix 8: ILCfile.m

```
clear all;
close all;
load ILCdata
F=zeros(401,1);
sim('ILCsim');

%Processensitivity
[nums,dens] = ss2tf(Ap,Bp,Cp,Dp);
P= tf(nums,dens);
[numc,denc] = ss2tf(ac,bc,cc,dc);
C=tf(numc,denc);
Sp=P/(1+P*C);

%pole-zero cancelation
Msys=minreal(Sp);
[numtf,dentf] = tfdata(Msys,'v');

%Discrete Processensitivity
[numd,dend] = c2dm(numtf,dentf,1e-3,'tustin');

%Determine the inverse Processensitivity
[ni,di,phd] = zpetc(numd,dend,1);

%plotting L and the Sp(discrete)
figure(1)
dbode(ni,di,1e-3);
hold on;
dbode(numd,dend,1e-3);

%Designing filter L en Q
LE=0;
for p=1:1:4
    Le=filter(ni,di,E);
    if p == 1
        figure(2);
        plot(T,E,'b');
        hold on;
        maxerror1= max(E)
    end
end

%Setting back the feedforward vector
extra=Le(length(Le),1)*ones(phd,1);
LL=[Le((phd+1):length(Le),1);extra];
LE=LE+LL;
FF=LE;
%filtering with Q
[Qnum,Qden] = butter(4,50/500);
F=filtfilt(Qnum,Qden,FF);
sim('ILCsim')
```

```
%plotting the error
figure(2);
if p == 1
    plot(T,E,'r');
end
if p == 2
    plot(T,E,'g');
end
if p >= 3
    plot(T,E,'k');
end

Title('Error after 4 iteration steps');
xlabel('Time in [s]');
ylabel('Error in [rad]');
hold on;
end
maxerror2= max(E)

%Testing convergencecriteria
Q=tf(Qnum,Qden);
L=tf(ni,di);
Spd=tf(numd,dend);
H=Q*(1-L*Spd);
[numh,denh]=tfdata(H,'v');
[Mc,Pc,Wc]=dbode(numh,denh,1e-3);
figure(3);
plot(Wc,abs(Mc));
Title('Convergence criterium');
ylabel('|Q(1-LSp)|');
xlabel('frequency [rad/s]');
```

Appendix 9: ILCsim.mdl

